Rare Metal Materials and Engineering
Volume 55, Issue 1, January 2026
Available online at www.rmme.ac.cn

Science Press

Cite this article as: Yang Laixia, Zhang Longbo, Xie Qidong, et al. Effects of CNTs Addition on Microstructure and Properties of Pure Copper Prepared by LPBF[J]. Rare Metal Materials and Engineering, 2026, 55(01): 27-34. DOI: https://doi.org/10.12442/j.issn.1002-185X.20240754.

ARTICLE

Effects of CNTs Addition on Microstructure and Properties of Pure Copper Prepared by LPBF

Yang Laixia[1], Zhang Longbo[1], Xie Qidong[2], Zhang Yanze[1], Yang Mengjia[1], Mao Feng[3], Chen Zhen[2]

[1] School of Mechanical Engineering, Xi'an University of Science and Technology, Xi'an 710054, China; [2] School of Mechanical Engineering, Xi'an Jiaotong University, Xi'an 710049, China; [3] Longmen Laboratory, Luoyang 471000, China

Abstract: Copper manufactured by laser powder bed fusion (LPBF) process typically exhibits poor strength-ductility coordination, and the addition of strengthening phases is an effective way to address this issue. To explore the effects of strengthening phases on Cu, Cu-carbon nanotubes (CNTs) composites were prepared using LPBF technique with Cu-CNTs mixed powder as the matrix. The formability, microstructure, mechanical properties, electrical conductivity, and thermal properties were studied. The result shows that the prepared composites have high relative density. The addition of CNTs results in inhomogeneous equiaxed grains at the edges of the molten pool and columnar grains at the center. Compared with pure copper, the overall mechanical properties of the composite are improved: tensile strength increases by 52.8% and elongation increases by 146.4%; the electrical and thermal properties are also enhanced: thermal conductivity increases by 10.8% and electrical conductivity increases by 12.7%.

Key words: laser powder bed fusion (LPBF); Cu-CNTs composites; mechanical property; thermal conductivity

1 Introduction

Pure copper is an important material with high electrical conductivity, which is 102% of the international annealed copper standard (IACS), and fine thermal conductivity of 400 W/(m·K), making it widely used in heat transfer and electromagnetic fields. However, current traditional manufacturing techniques are unable to produce fine parts with complex geometric structures. As a result, metal additive manufacturing processes, especially laser powder bed fusion (LPBF), have attracted significant attention due to their ability to fabricate geometrically complex parts from powder materials[1–4]. Combining the advantage of LPBF with the high thermal conductivity of pure copper, parts with higher heat transfer efficiency can be produced[5]. However, due to the high laser reflectivity of copper to infrared radiation, especially that within the range of 1060 – 1080 nm which corresponds to the near-infrared radiation of the most commonly used lasers in LPBF, and extremely high thermal conductivity (a small amount of heat can be absorbed by the instantaneous dissipation) [6], the strength and density of the prepared samples generally cannot meet the practical application requirements.

Currently, an effective method is to add other strengthening phases into the copper matrix to enhance its strength. For this purpose, many researchers prefer pre-alloyed copper powder, which has slightly lower optical reflectivity than pure copper. This enables the production of dense parts using alloys such as Cu-Cr[7], Cu-Cr-Zr[8], Cu-Sn[9], and Cu-Zn[10]. Therefore, these alloy samples exhibit significantly improved density and much higher tensile strength compared to as-built pure copper parts. The addition of other metal elements with lower thermal conductivity seriously hinders the transmission of phonons and electrons, resulting in much lower thermal and electrical conductivities compared to those of pure copper samples[11]. Currently, nanoparticle-reinforced metal matrix composites have been proven to be one of the promising materials to

Received date: January 20, 2025
Foundation item: National Key Research and Development Program of China (2023YFB4606400); Supported by Longmen Laboratory Frontier Exploration Topics (LMQYTSKT003)
Corresponding author: Chen Zhen, Ph. D., Associate Professor, School of Mechanical Engineering, Xi'an Jiaotong University, Xi'an 710049, P. R. China, E-mail: chenzhen2025@xjtu.edu.cn

address this challenge[12]. A new trend has emerged: adding nanomaterials with higher laser absorption and electrical conductivity to copper powder particles, and then using LPBF technique to prepare composites with high strength, thermal conductivity, and electrical conductivity. Therefore, this study used nanoscale carbon nanotubes (CNTs) covering on the surface of pure copper powder to prepare samples with enhanced laser absorption, strength, electrical conductivity, and thermal conductivity. Although the idea of copper powder coated with CNTs has been previously proposed[13], LPBF behavior and the resulting mechanical properties and thermal conductivity have seldom been reported.

Consequently, this study proposed an alternative method involving mixing CNTs with copper powder particles to improve the powder's laser absorption and LPBF behavior. The effects of CNTs on the formability, microstructure, mechanical properties, electrical conductivity, and thermal conductivity of the composites were evaluated.

2 Experiment

The gas-atomized copper powder (99.96% purity, D_{50}: 37.87 μm, Asia New Materials Co., Ltd, China) and multi-walled CNTs (diameter: 4 – 6 nm, Jiangsu Xianfeng Nanomaterials Technology Co., Ltd, China) were used as the initial materials. 0.3wt% CNTs were dispersed in anhydrous ethanol. A beaker containing this solution was placed in a water bath, with the probe of an ultrasonic homogenizer immersed in the solution. The solution was subjected to ultrasonic homogenization until the CNTs were evenly dispersed. Pure copper powder was added to the solution, and the mixed solution was evenly stirred using a vacuum homogenizer (ZYMC-200V). Powder mixing process was carried out in three modes of variable-speed rotation: 1500 r/min for 20 s, 2500 r/min for 30 s, and 1000 r/min for 15s. The particle size distribution of the Cu-0.3wt% CNTs mixed powder was measured by an LS-909 laser diffraction particle size analyzer (Omec, China) in wet mode. Before the LPBF process, the powder was dried in a vacuum drying oven at 120 °C for 10 h. Vacuum drying not only removed moisture from the powder to enhance its fluidity, but also effectively prevented oxidation of the Cu-0.3wt% CNTs mixed powder during the LPBF process.

The optical reflectance of the powder was measured at room temperature using a UV-visible near-infrared spectrophotometer (Shimadzu UV3600; Agilent CARY 300; PE lambda 750S). Measurements were performed in total reflection mode, with a 100% reflectance as the reference material. Light absorption was calculated from the reflectance data using the formula: light absorption (%) =100% − light reflection (%).

LPBF was performed using a machine developed by the Department of Mechanical Engineering of Xi'an Jiaotong University. Throughout the fabrication process, oxygen levels in the build chamber were maintained below 0.01vol% by purging with protective argon gas. The fiber laser of the device was operated at a wavelength range of 1060–1080 nm. First, an STL file for a cube part with dimensions of 8 mm×8 mm× 8 mm was created using Magics software (Materialise, Belgium). All cube parts were fabricated on a stainless steel substrate under various LPBF process parameters. The density of these parts was measured via the Archimedes method, and the relative density was calculated using a theoretical (true) density of 8.87 g/cm^3. The theoretical (true) density of the Cu-0.3wt% CNTs composite powder was determined using a Multipycnometer (Quantachrome Instruments). In addition, all LPBF experiments were conducted without preheating the build plate.

The printing adopted a segmented scanning strategy: each segment of the layer was 6 mm in length, and the laser beam was rotated 67° for each subsequent layer during scanning. The LPBF parameters yielding the highest part density (laser power: 380 W; scanning speed: 230 mm/s; hatch spacing: 0.1 mm) were selected and kept consistent for fabricating both pure Cu and Cu-CNTs composite samples. These parameters were used to manufacture dog-bone samples for mechanical property testing.

The microscopic morphology of the sample was observed using a JEM-IT500 tungsten filament scanning electron microscope (SEM, JEOL, Japan). Phase analysis was performed via X-ray diffractometer (XRD, Bruker D8 ADVANCE, Germany) with a scanning angle ranging from 10° to 90°.

The test data were processed and analyzed using MDI JADE6.0 software. The grain orientation and texture of the samples were characterized by electron backscatter diffractometer (EBSD) using a JSM-7900F field emission SEM (JEOL, Japan), and then the data were processed using Channel 5 software. To evaluate the mechanical properties, dog-bone tensile samples (dimensions: 10 mm×5 mm×2 mm) were printed according to GB/T 228.1-2010 standard, as shown in Fig. 1a. Tensile tests were performed at a rate of 1 mm/min using an Instron M4206 testing machine. Thermal conductivity was measured using a calorimeter (Hot Disk2500s) on printed samples with dimensions of 10 mm×10 mm×2 mm, as shown in Fig.1b.

3 Results and Discussion

3.1 Formability

The particle size, microscopic morphology, laser absorptivity, and Raman spectrum of the Cu-CNTs mixed powder are shown in Fig. 2. As shown in Fig. 2d, the median particle size (D_{50}) of the mixed powder is 38.83 μm, which

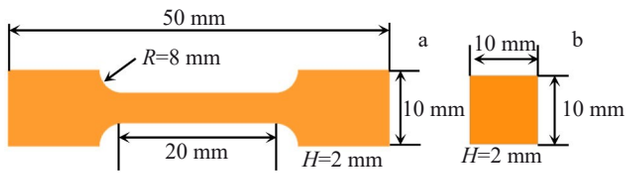

Fig.1 Schematic diagrams of tensile sample (a) and thermal conductivity test sample (b)

satisfies the powder size requirement (13–53 μm) for LPBF technique. Fig.2c reveals that the sphericity of the Cu powder is well maintained during the preparation of the mixed powder, with no degradation observed during the preparation process. The basic structure of CNTs dispersed by ultrasonic waves is not seriously damaged. In the wavelength range of 1060–1080 nm (Fig. 2e), the laser absorption rate of the Cu-CNTs mixed powder reaches 48.7%, compared to that of pure Cu powder (23.4%), representing a 108.1% increment. It suggests that the addition of CNTs significantly enhances the light absorption of copper powder, which is attributed to the high optical absorption of carbon materials in the infrared region. Fig.2f shows that the Raman spectral characteristics of the mixed powder are not significantly altered compared to those of the original CNTs. The I_{D_0}/I_{G_0} ratio of the original CNTs is 1.173, while the I_{D_1}/I_{G_1} ratio of the water-bath ultrasonically homogenized CNTs is 1.211, indicating only a 3.24% reduction in structural integrity, and confirming that water-bath ultrasonic homogenization effectively preserves the structural integrity of CNTs. The I_{G_0}/I_{2D_0} ratio of the original CNTs is 2.467, and the I_{G_1}/I_{2D_1} ratio of the ultrasonically homogenized CNTs in water bath is 2.491. The I_{2D} value is closely related to the number of CNT layers, and the increase in the abovementioned ratio indicates that the water-bath ultrasonic homogenization leads to a slight increase in the number of CNT layers. This is because during the ultrasonic homogenization process, some dispersed thin-layer CNTs may undergo mild agglomeration or interlayer re-combination. Calculations show that the number of layers of water-bath ultrasonically homogenized CNTs increases by 0.97%, compared with that of the original CNTs. Considering the change in the I_D/I_G ratio, CNTs after ultrasonic homogenization can still maintain their structural integrity.

Cu-CNTs composites are successfully fabricated under the specified process parameters, which include a laser power of 380 W, a scanning speed of 230 mm/s, a scanning spacing of 0.1 mm, and a powder layer thickness of 0.03 mm. The density of the Cu-CNTs composites is 96.6%, while that of the pure Cu is 92.3%. The corresponding optical images are shown in Fig. 3c and 3d. There are noticeable pores and a

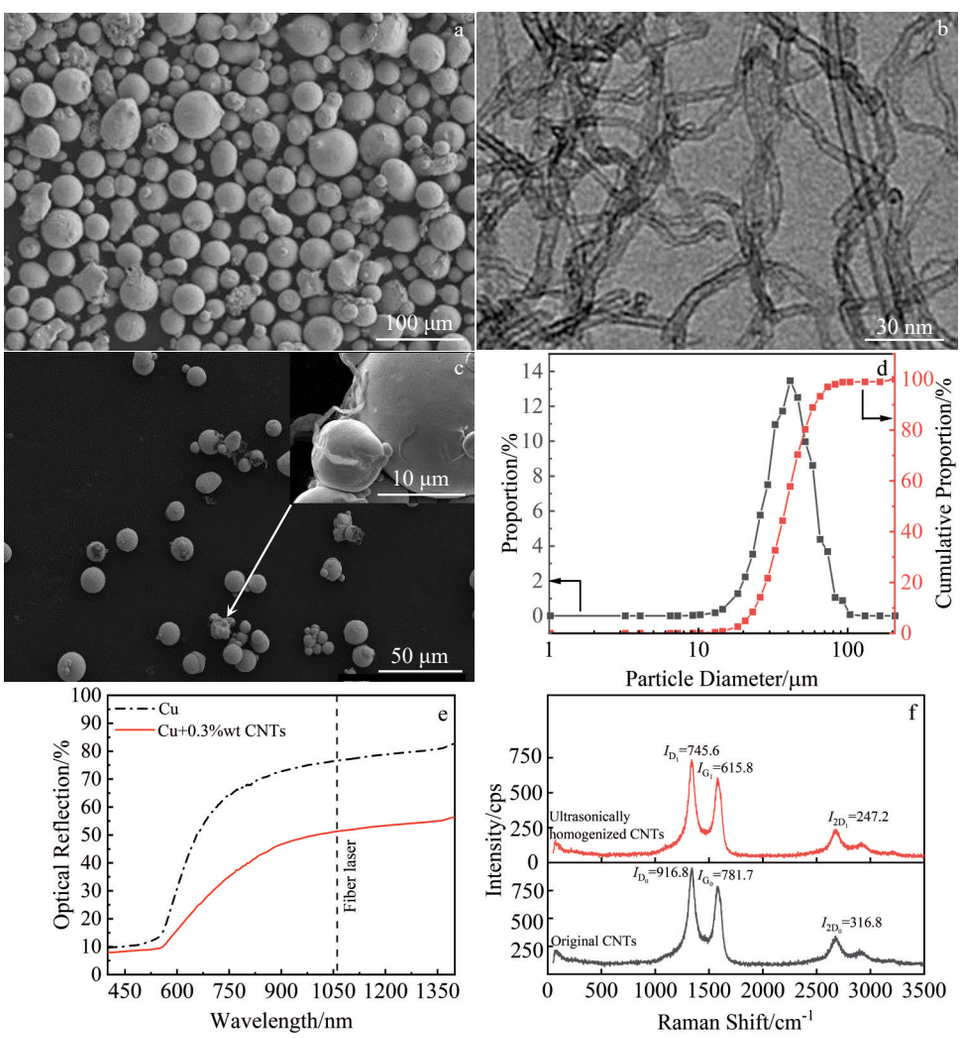

Fig.2 Microscopic morphologies of initial Cu powder (a), initial CNTs (b), and Cu-CNTs mixed powder (c); particle size distribution of Cu-CNTs mixed powder (d); optical reflection of pure Cu powder and Cu-0.3%wt CNTs in wavelength range of 400–1400 nm (e); Raman spectra of original CNTs and ultrasonically homogenized CNTs (f)

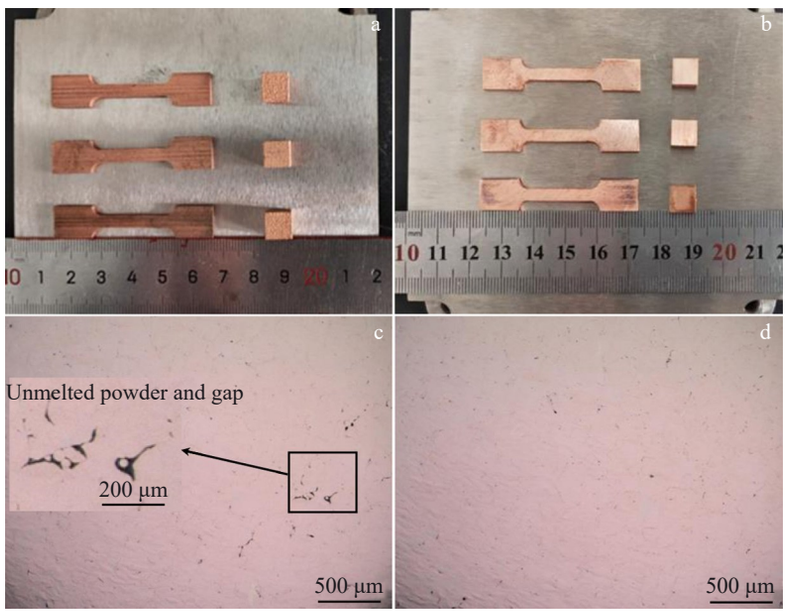

Fig.3 Macroscopic morphologies (a–b) and defect diagrams (c–d) of prepared pure Cu (a, c) and Cu-CNTs composite (b, d) samples

negligible amount of unmelted powder in the pure Cu sample, as indicated in the magnified image in Fig.3c. The presence of unmelted powder is attributed to the low laser absorption rate of pure Cu powder: most of the laser energy is reflected, leaving only a small portion of energy for sample fabrication. Consequently, the powder between adjacent molten pools is less likely to melt, leading to an increase in defect. However, due to the incorporation of CNTs which have a higher laser absorption rate, more energy is used in the fabrication of Cu-CNTs composite samples. This results in a significant reduction in surface defects and virtually eliminates unmelted powder. Consequently, with the addition of CNTs, the non-melting phenomenon of the powder is eliminated, and the number of pores is also reduced.

3.2 Microstructure

As observed in XRD patterns (Fig. 4a), the addition of CNTs to pure Cu does not result in the formation of impurity phases with Cu during the fabrication process. Meanwhile, Raman spectrometer was used to test the prepared samples, and the resulting spectra are shown in Fig. 4b. There is no characteristic peak of CNTs in the Raman spectrum of pure Cu sample, whereas the Cu-CNTs composite sample exhibits an obvious G-band. During LPBF process, CNTs are surrounded by molten metal and covered by the solidified metal matrix, which may affect Raman scattering results. Therefore, the Cu-CNTs composite samples show a pronounced G-band peak, which corresponds to the vibration of carbon-carbon bonds within CNTs. This confirms the retention of CNTs in the prepared composite samples.

The grain morphology and size were analyzed through large-area EBSD with a step size of 0.9 μm, and the grain boundary angular orientation is depicted in Fig. 5. In inverse pole figures (IPFs), as shown in Fig. 5a – 5b, the regions of equiaxed grain (EG) and columnar grain (CG) are distinguishable. Specifically, CG refers to the CG region, and EG indicates the EG region. According to IPFs, the grain of the prepared sample exhibits no obvious preferred orientation. The CNTs content significantly influences the grain morphology of pure Cu samples.

As illustrated in Fig.5a, CGs predominantly grow along the reverse direction of heat flow (i. e., from the molten pool

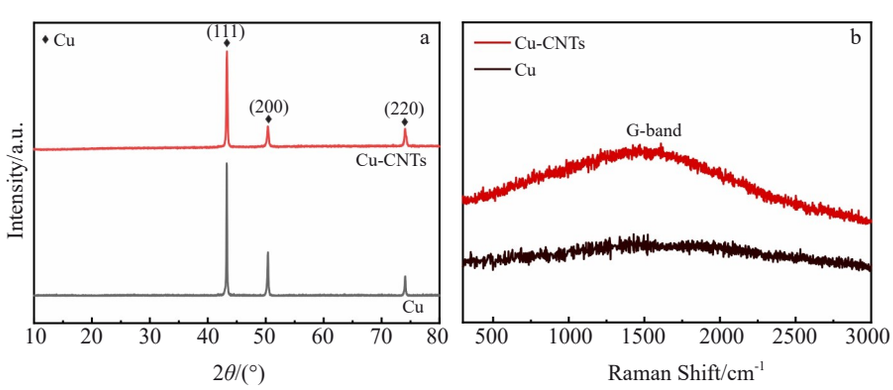

Fig.4 XRD patterns (a) and Raman spectra (b) of pure Cu and Cu-CNTs composite samples

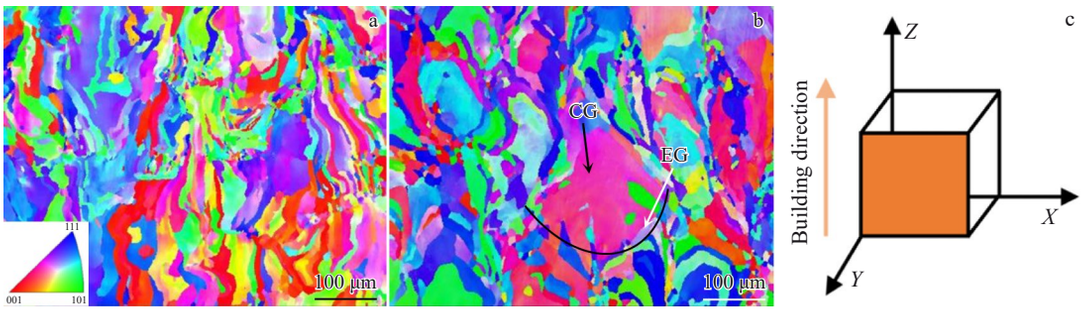

Fig.5 IPFs of pure Cu (a) and Cu-CNTs composite (b) samples; schematic diagram of test surface marked by orange area (c)

boundary to the center), while EGs are randomly distributed along the molten pool boundary and within the molten pool. However, upon adding CNTs to the pure Cu samples, the grains exhibit distinct differentiation in terms of shape and size: EGs at the edge of the molten pool and coarse CGs at the center of the molten pool, as indicated by the black arrow in Fig.5b.

As depicted in Fig. 5a, EGs are initially randomly distributed within the pure Cu sample. After incorporating CNTs into the pure Cu sample, EGs start to accumulate near the edge of molten pool. This phenomenon promotes the formation of a greater number of coarse CGs with similar orientations, which ultimately coalesce into larger CGs.

The influence of CNTs on grain morphology may be attributed to their high thermal conductivity, which modifies the heat transfer dynamics within the molten pool. The impact of CNTs on the microstructure is illustrated in Fig. 6. The overall microstructure of the sample fabricated using LPBF is comparable to that of the pure Cu sample, as depicted in Fig. 6a. Owing to the well-oriented thermal gradient and an inherent characteristic of LPBF which facilitates epitaxial growth, the grains within the molten pool are predominantly columnar, with a few EGs distributed relatively uniformly. However, for the composite samples, the EGs distributed at the molten pool boundary are in contact with the solidification zone, where heat dissipation is the most rapid, leading to swift quenching. Consequently, the grains at the boundary of the molten pool typically form as EGs.

Drawing upon the nucleation sites supplied by CNTs, the elevated cooling rate of composites enhances the number of nucleation events and the rate of heterogeneous nucleation[14]. A higher cooling rate results in a faster solidification rate, thereby restricting grain growth. The absorption of laser energy, coupled with the swift solidification at the heterogeneous nucleation sites, contributes to the formation of EGs with a random orientation at the periphery of the molten pool[15].

However, the grain size in the composite is increased with the introduction of CNTs. This can be attributed to the higher temperatures in the center of the molten pool compared to its edges, leading to overheating of the molten metal and the melting of some initial nucleation sites, thus restricting nucleation rates and providing longer time for grain growth. This elucidates the disparity in grain morphologies between the center and the periphery of the molten pool.

Moreover, CNTs exert an influence on the alteration of heat transfer dynamics within composites. Typically, in LPBF, the heat flow proceeds from the center of the molten pool toward the boundary, as indicated by red arrows in Fig. 6a. Incorporating CNTs can improve heat transfer rates and temperature gradients, thereby promoting the formation and growth of CGs. Consequently, CGs sharing similar orientations amalgamate into larger and coarser CGs, as shown in Fig.6b.

Regarding the pure Cu sample, CGs grow in a direction opposite to the heat flow direction. Upon the addition of CNTs to the material, the thermal conductivity and cooling rate of the composite both increase. This makes it easier to form EGs at the edge of the molten pool, whereas the center of the

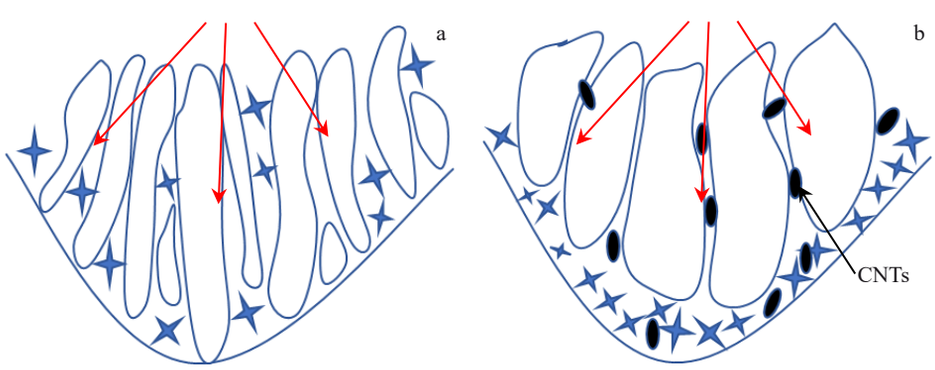

Fig.6 Schematic diagrams of effect of CNTs on microstructures of pure Cu (a) and Cu-CNTs composite (b) samples

molten pool tends to form CGs due to the well-aligned temperature gradient. Heat transfer is facilitated in the vicinity of CNTs which possess high thermal conductivity. Within the composite samples, CNTs constitute a larger portion of the heat transfer pathways in the molten pool, thereby promoting the formation of numerous longer CGs with similar orientations. These grains amalgamate to form larger grains. Hence, incorporating CNTs leads to a heterogeneous microstructure in the Cu-CNTs composites.

CNTs also exert a significant influence on the distribution of recrystallized structure within the composites. As illustrated in Fig. 7a – 7b, the deformed microstructure of Cu-CNTs samples is notably more pronounced than that of pure Cu samples. This is attributed to the nanoscale fibrous nature of CNTs. During the formation process, grains at the molten pool boundary are in contact with the solidification zone, where heat dissipation is accelerated and rapid quenching ensues. This leads to an increase in EGs and a rise in dislocation density among EGs, thereby rendering recrystallization more difficult. In summary, the enhancement of the deformed microstructure optimizes the mechanical properties of the material, enabling it to better withstand high loads and pressures. Moreover, the substructures generated within the grain become more intricate, contributing to the overall enhancement of the material's properties. The increased content of deformed structures elevates the dislocation density, accelerating the material's recovery rate in subsequent heat treatment processes to a certain extent, and aiding in the reduction of material processing time.

3.3 Mechanical properties

As listed in Table 1, the pure Cu sample exhibits a tensile strength of 145.7 MPa and an elongation of 11.2%, while the Cu-CNTs composite sample demonstrates a tensile strength of 222.6 MPa and an elongation of 27.6%. In contrast, the addition of CNTs results in a 52.8% increment in the tensile strength and a 146.4% increase in elongation for the composite.

In the tensile curves shown in Fig. 8, the stress declines under the condition of minimal strain. This phenomenon occurs because the two samples are not fully dense, containing defects such as microcracks and microholes. Local deformation occurs at the initial stage of loading, resulting in a slight decrease in stress.

The improved tensile properties of composites may be due to the following strengthening mechanisms. Orowan strengthening and load transfer strengthening are strongly dependent on the volume fraction of CNTs. For composites containing CNTs with a high aspect ratio, the primary strengthening mechanism is load transfer[16–17]. Given the presence of CNTs in composites, Orowan strengthening may have a significant strengthening effect on Cu-CNTs composites.

Grain boundary strengthening, also known as Hall-Petch strengthening, is closely related to the average grain size. However, according to the EBSD grain data in Fig. 5, the average grain size of the Cu-CNTs sample is relatively larger. Therefore, grain boundary strengthening is unlikely to be one of the main strengthening mechanisms. In addition, the addition of CNTs and the heterogeneous structure induced by CNTs unlikely contribute to a back-stress strengthening mechanism during the deformation of Cu-CNTs composites, which improves the strength and plasticity of the materials[18–20].

The fracture morphology of Cu-CNTs composites prepared by the LPBF method is shown in Fig. 9b, revealing a significant influence of CNTs on the fracture morphology of samples. It can be seen from Fig. 9a that the tensile fracture surface of pure Cu sample shows a large number of cleavage planes alongside a small number of dimples. The low elongation of this sample is attributed to quasi-cleavage fracture and the presence of large defects. In contrast, Fig. 9b shows that the tensile fracture morphology of Cu-CNTs composites is characterized by a high density of dimples, with small dimples distributed within the large ones. This observation demonstrates that the tensile strength and elongation of Cu-CNTs composites are significantly improved compared with pure Cu samples. This is because the addition of CNTs increases the material's energy absorption capacity: more energy is used to melt the metal powder, resulting in a reduction in the number of internal defects and pores. Therefore, during the tensile process, dislocations accumulate at the grain boundaries, inducing stress concentration that causes interface debonding and formation of tiny cavities. The material between these cavities is stretched, resembling a protrusion. The cavities connect to form dimples, which makes the composite more resistant to fracture. However, the defects in pure Cu samples are relatively larger. When stress concentration occurs due to

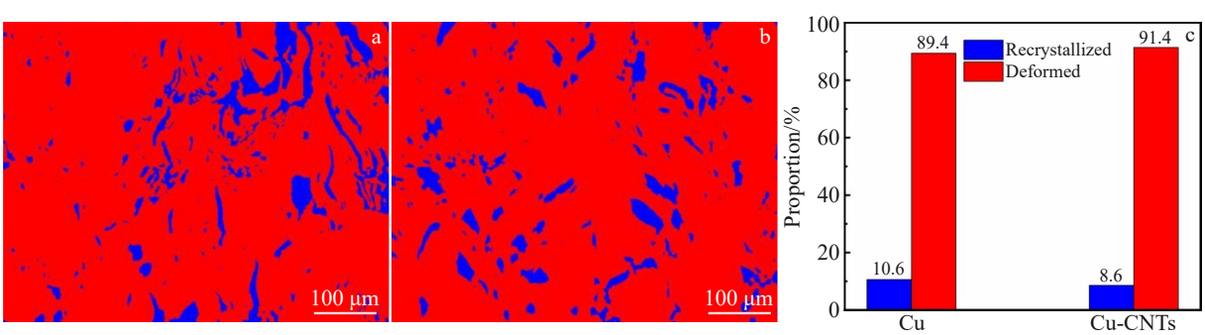

Fig.7 Recrystallized structures of pure Cu (a) and Cu-CNTs composite (b) samples; proportions of recrystallized and deformed grains (c)

Table 1 Tensile properties of pure Cu and Cu-CNTs composite samples

Sample	Tensile strength/MPa	Elongation/%
Cu	145.7	11.2
Cu-CNTs	222.6	27.6

the accumulation of dislocations at the grain boundaries during the stretching process, microcracks tend to form at these defects and propagate rapidly, making the material easier to fracture.

3.4 Thermal conductivity

Table 2 summarizes the thermal conductivity of the pure Cu and Cu-CNTs composite samples. The results show that the thermal conductivity of Cu-CNTs composite sample is higher. Compared with that of pure Cu sample, the thermal conductivity of Cu-CNTs composite sample increases from 405.54 W/(m·K) to 449.34 W/(m·K), representing an increase of 10.8%. Similarly, the thermal diffusion increases from 120.96 mm^2/s to 134.97 mm^2/s, showing an increment of 11.6%. The specific heat capacity decreases from 0.41 J/(g·K) to 0.39 J/(g·K), inferring a reduction of 4.9%. The electrical conductivity of parts was theoretically calculated using Wiedemann-Franz law. With the Lorentz constant L=2.44×10^{-8} W· Ω/K^2[21] and temperature T=300 K, the calculated electrical conductivity is 6.2×10^7 S/m. Compared with that of the pure Cu sample, the electrical conductivity of Cu-CNTs composite sample is increased from 5.5×10^7 S/m to 6.2×10^7 S/m, increasing by 12.7%.

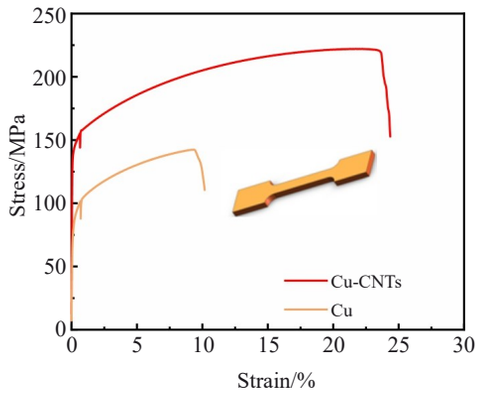

Fig.8 Stress-strain curves of pure Cu and Cu-CNTs composite samples at room temperature

CNTs, due to their nanostructure and high aspect ratio, provide highly efficient pathways for phonon and electron transport. Their carbon-carbon bonding endows the material with excellent thermal and electrochemical stability, resulting in extremely high thermal and electrical conductivities[22]. When added to Cu matrix materials, CNTs retain these high thermal and electrical conduction properties. Dispersed CNTs partially replace the Cu-based thermal conduction network in the matrix, forming a new network with enhanced thermal conductivity. Compared to the thermal conductivity of pure Cu matrix, this new thermal conduction network exhibits superior phonon and electron transport capabilities. Thus, the addition of CNTs significantly enhances the thermal conductivity of the Cu material.

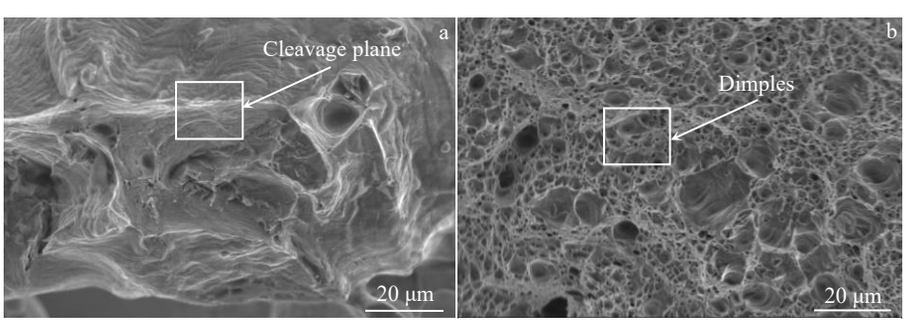

Fig.9 Tensile fracture morphologies of pure Cu (a) and Cu-CNTs composite (b) samples

Table 2 Thermal diffusivity, thermal conductivity, specific heat capacity, and electrical conductivity of pure Cu and Cu-CNTs composite samples

Sample	Thermal diffusivity/$mm^2·s^{-1}$	Thermal conductivity/$W·(m·K)^{-1}$	Specific heat capacity/$J·(g·K)^{-1}$	Electric conductivity/×10^7 $S·m^{-1}$
Cu	120.96±0.06	405.54±0.20	0.41±0.01	5.5
Cu-CNTs	134.97±0.89	449.34±2.97	0.39±0.01	6.2

4 Conclusions

1) Ultrasonic homogenization in water minimizes structural damage to CNTs, and the addition of CNTs enhances the laser absorption rate of the composites. Under the optimal parameter combination, Cu-CNTs composites are successfully fabricated by the LPBF method, with the density of 96.6%.

2) Due to their high thermal conductivity, CNTs can alter the heat transfer behavior and cooling rate of the composite material. CNTs also modify the local temperature gradient, leading to the formation of EGs at the edge of the molten pool

and CGs in the center, and resulting in heterogeneous structure.

3) The Cu-CNTs composite exhibits a tensile strength of 222.6 MPa and an elongation of 27.6% at room temperature.

4) The prepared Cu-CNTs composite sample achieves a thermal conductivity of 449.34 W/(m·K) and an electrical conductivity of 6.2×10^7 S/m.

References

1 Wu Jiahao, Xu Feng, Wang Huanle *et al*. *Rare Metal Materials and Engineering*[J], 2024, 53(7): 1953 (in Chinese)

2 Zhao Yanchun, Song Haizhuan, Ma Huwen *et al*. *Rare Metal Materials and Engineering*[J], 2024, 53(1): 102 (in Chinese)

3 Fan Yongxia, Lin Yan, Ao Qingbo *et al*. *Rare Metal Materials and Engineering*[J]. 2023, 52(10): 3630 (in Chinese)

4 Wu Jiahao, Xu Feng, Wang Huanle *et al*. *Rare Metal Materials and Engineering*[J], 2024, 53(7): 1953 (in Chinese)

5 Zhao Yanchun, Song Haizhuan, Ma Huwen *et al*. *Rare Metal Materials and Engineering*[J], 2024, 53(1): 102

6 Fan Yongxia, Lin Yan, Ao Qingbo *et al*. *Rare Metal Materials and Engineering*[J], 2023, 52(10): 3630 (in Chinese)

7 Zhang Shasha, Zhu Haihong, Zhang Luo *et al*. *Materials Letters*[J], 2019, 237: 306

8 Christopher W, Bruno B. *Materials Science and Engineering A*[J], 2019, 744: 215

9 Matías S, Magdalena W, Jorge R. *Optics and Lasers in Engineering*[J], 2018, 100: 1

10 Zhang Shasha, Zhu Haihong, Hu Zhiheng *et al*. *Powder Technology*[J], 2019, 342: 613

11 Suraj D J, Jozef V, Jean-Pierre K *et al*. *Material Design & Processing Communications*[J], 2019, 2(2): e94

12 Riccardo C, Maurizio V. *Metals*[J], 2014, 4(1): 65

13 Suraj D J, Sasan D, Jozef V *et al*. *Materials*[J], 2019, 12(15): 2469

14 Prasad A, Yuan L, Lee P *et al*. *Acta Materialia*[J], 2020, 195: 392

15 Mohammad R J, Hesam P, Vahid F *et al*. *Materials Characterization*[J], 2022, 192: 112206

16 Park J G, Keum D H, Lee Y H. *Carbon*[J], 2015, 95(3): 690

17 Liu Z Y, Xiao B L, Wang W G *et al*. *Carbon*[J], 2012, 50(5): 1843

18 Wang Y M, Voisin T, McKeown J T *et al*. *Nature Materials*[J], 2018, 17: 63

19 Xu Run, Fan Genlian, Tan Zhanqiu *et al*. *Materials Research Letters*[J], 2018, 6: 113

20 Wang Zihong, Lin Xin, Kang Nan *et al*. *Additive Manufacturing*[J], 2020, 34: 101260

21 Sebastian J R, Ralf G, Matthias A L *et al*. *Advanced Engineering Materials*[J], 2016, 18(9): 1661

22 Valentin N P. *Materials Science and Engineering R*[J], 2004, 43: 61

添加 CNTs 对激光粉末床熔融纯铜的微观结构和性能的影响

杨来侠[1]，张龙博[1]，谢启东[2]，张晏泽[1]，杨蒙佳[1]，毛　峰[3]，陈　祯[2]

(1. 西安科技大学 机械工程学院，陕西 西安 710054)

(2. 西安交通大学 机械工程学院，陕西 西安 710049)

(3. 龙门实验室，河南 洛阳 471000)

摘　要：激光粉末床熔融（LPBF）工艺制造铜通常表现出较差的强度-塑性配合，添加增强相是改善这种配合的有效方法。为了探究增强相对Cu的影响，以Cu-碳纳米（CNTs）混合粉末为基体，采用LPBF技术制备了Cu-CNTs复合材料，研究了其成形性能、微观结构、力学性能、导电性能和热性能。结果表明，所制备的复合材料具有较高的相对密度。CNTs的加入导致了熔池边缘等轴晶粒和中心柱状晶粒的不均匀。与纯铜相比，复合材料的整体力学性能得到改善（抗拉伸强度提高52.8%，伸长率提高146.4%），导电性能和热性能也得到提高（导热系数提高10.8%，电导率提高12.7%）。

关键词：激光粉末床熔融（LPBF）；Cu-CNTs复合材料；力学性能；热导率

作者简介：杨来侠，女，1961年生，博士，教授，西安科技大学机械工程学院，陕西 西安 710054，E-mail：yanglx@xust.edu.cn